Available online at www.CivileJournal.org

Civil Engineering Journal

(E-ISSN: 2476-3055; ISSN: 2676-6957)

Vol. 11, No. 06, June, 2025

Examining the Erosion Resistance of Cement-Bentonite Barriers: Effects of Confining Pressure and GGBS Content

Muhammad A. Walenna [1*], Alexander Royal [2], Ian Jefferson [2], Gurmel Ghataora [2], Tri Harianto [1], Ardy Arsyad [1], Zarah A. Hanami [3]

[1] *Department of Civil Engineering, Faculty of Engineering, Universitas Hasanuddin, Gowa 92171, Indonesia.*

[2] *Department of Civil Engineering, School of Engineering, University of Birmingham, Edgbaston B15 2TT, United Kingdom.*

[3] *Department of Environmental Engineering, Faculty of Engineering, Universitas Hasanuddin, Gowa 92171, Indonesia.*

Received 25 January 2025; Revised 07 May 2025; Accepted 15 May 2025; Published 01 June 2025

Abstract

This study investigates the erosion resistance of cement-bentonite (CB) barriers, focusing on the role of varying levels of Ground Granulated Blast Furnace Slag (GGBS) content and confining pressure, crucial for infrastructure such as dams and levees. Employing a bespoke modified triaxial erosion testing setup, the research assesses how different confining pressures, GGBS proportions, and curing periods impact the erosion resistance of CB materials under varying stress conditions. Results demonstrate that increasing GGBS proportions enhances erosion resistance by improving the CB matrix microstructure, while higher confining pressures generally increase resistance. However, combinations of high confining pressure and erosive force can lead to barrier material failure, with buckling failure occurring at elevated pressures (100 kPa and above), highlighting a trade-off between enhancing erosion resistance and maintaining structural stability. Extended curing periods allow for material strength development, enhancing stability, yet delayed erosion phases at higher confining pressures and longer curing durations suggest gradual crack formation, potentially leading to hydraulic fracturing. This underscores the need for meticulous design considerations regarding load conditions due to significant failure modes such as buckling. The findings emphasize that the strategic combination of GGBS content, confining pressure, and curing period is crucial in optimizing barrier performance, highlighting the importance of selecting optimal material formulations and operational parameters to maximize erosion resistance and ensure the longevity and safety of civil engineering structures.

Keywords: Internal Erosion; Barrier Materials; Cement-Bentonite; GGBS; Confining Pressures.

1. Introduction

Cement-bentonite mixtures have been increasingly recognized as indispensable materials in civil engineering due to their distinctive combination of low permeability, plasticity, and durability, making them ideally suited for seepage control systems and cutoff walls in dams, levees, and other hydraulic structures [1-3]. From a chemical standpoint, bentonite typically contains silica, alumina, and water [4], and it is extensively employed to improve both the mechanical characteristics and durability of cement-based materials. Its high pozzolanic reactivity promotes additional C-S-H gel formation through the consumption of portlandite [5, 6], which in turn strengthens the cementitious matrix and improves resistance against environmental degradation. Furthermore, both raw and calcined bentonite have demonstrated an ability to lower bulk density while simultaneously increasing compressive

* Corresponding author: mawalenna@unhas.ac.id

http://dx.doi.org/10.28991/CEJ-2025-011-06-08

strength, Vickers hardness, and resistance to acidic environments [7-10]. Consequently, these observed enhancements suggest that cement-bentonite mixtures can serve as a reliable choice for improving the longevity and resilience of critical civil engineering structures.

Although cement-bentonite barriers are widely used for seepage control in dams and levees, numerous studies highlight their susceptibility to hazards that can compromise their long-term performance [11, 12]. For instance, hydraulic fracturing may occur when fluid pressures exceed the soil's tensile strength, principal effective stress, or stress conditions, leading to fracture development [11]. Additionally, the upper portion of the barrier is exposed to atmospheric conditions such as evaporation and infiltration, which can be intensified by climate change and result in repeated drying-wetting cycles that alter the barrier's hydraulic properties and diminish its overall effectiveness [12]. While seepage barriers generally excel at regulating water flow, they remain prone to cracks or fissures caused by fluctuations in pore pressure and steep hydraulic gradients, which concentrate seepage forces within and around the barrier [13]. The likelihood of cracking is further increased by greater tensile strain [14, 15]. In concrete-face rockfill dams constructed on alluvial foundations, concrete cutoff walls act as essential seepage control measures; however, they are exposed to complex loading conditions that can produce damage or cracking through interactions with foundation deformations and seepage effects [16]. Preserving the integrity of cement-bentonite cutoff walls becomes especially challenging in aggressive environments, where cyclic wetting-drying can lead to desiccation and cracking [17]. Once cracks are present, they can facilitate internal erosion, emphasizing the importance of hydraulic conditions, material properties, and stress states for maintaining barrier stability [18]. Although the potential for erosion in cement-bentonite barriers has been identified, existing research on these mechanisms remains limited, suggesting a need for further studies to protect not only the integrity of the barriers themselves but also the safety of the dam and surrounding communities.

In addition to these well-known vulnerabilities, recent case studies underscore the impact of bentonite content, seepage gradients, and long-term erosion mechanics in cutoff walls. For instance, Chowdhury et al. [19] reported that soil-bentonite (SB) cutoff walls with insufficient bentonite content can become susceptible to internal erosion or "plucking" over time, even if short-term hydraulic conductivity tests are passed. They recommend specifying a minimum 3% bentonite by weight to bolster long-term resilience of open-trench cutoff walls. Meanwhile, under variable flow conditions, Zhang et al. [20] found that the erosion rate increases with seepage gradient and that higher water velocities significantly accelerate internal erosion, particularly under steady flow. Under oscillatory flow, seepage still promotes erosion, albeit more slowly, yet once velocity surpasses a threshold, erosion can advance more rapidly. Relatedly, natural geologic heterogeneities compound erosion uncertainties; Zhao et al. [21] observed that preexisting voids and the unpredictable positioning of seepage channels in landslide dams can lead to localized erosion pathways, even when outlet elevations appear favorable.

Beyond erosive concerns, mechanical compatibility of the cutoff material is also critical. Pereira [22] emphasizes that the stiffness and strength of the barrier must be balanced against the surrounding soil to reduce stress concentrations while still resisting differential hydraulic pressure. Innovations in material formulations can further mitigate these vulnerabilities. For example, Wang et al. [23] highlighted that polymer-modified bentonite can resist crack formation under multiple wet–dry cycles with various contaminants, thanks to clogging mechanisms and cation scavenging effects. In the context of broader hydraulic structures, Alrowais et al. [24] demonstrated numerically that strategically placing and angling cutoff walls, particularly at the upstream heel, significantly reduces uplift pressure and, by extension, potential erosion threats.

Previous investigations into the erodibility of seepage barriers have largely been carried out under controlled laboratory conditions, often neglecting the broader range of environmental influences and long-term behavior encountered in actual site conditions. As early as 1985, Beier and Strobl observed that environmental factors could alter the pore water chemistry of cement-bentonite mixtures, triggering calcium leaching and thereby affecting their erosion resistance [25]. However, these preliminary findings offered limited justification for how such environmental conditions could surpass erosive forces in driving barrier degradation. Building on this, subsequent studies by Braithwaite [26], Alonso et al. [27] and Wang et al. [28] examined the erosion characteristics of cement-bentonite in similarly constrained laboratory environments with narrow erosive force ranges, focusing on raw bentonite and additive materials such as GGBS. Garand et al. [29] extended the research to related materials like plastic concrete using Controlled Water Velocity apparatus, demonstrating minimal erosion under high hydraulic heads; yet, the strict lab-based approach may not fully represent field conditions. Similarly, Walenna et al. [30] assessed how barrier materials respond to hydraulic pressures and environmental stresses but conducted only limited testing on specific mixtures and curing periods, revealing a significant knowledge gap regarding the influence of variable curing times. Collectively, these studies underscore the need for more comprehensive investigations that capture a wider spectrum of real-world scenarios, including different stages of curing and a broader range of erosive and environmental forces, to better predict and enhance the long-term stability of seepage barriers. Comprehensive research on internal erosion, summarized in Table 1, indicates a significant exploration into the erosion resistance and behavior of various soil materials under controlled testing conditions.

Table 1. Summary of Past Studies on Erosion Resistance and Testing Methodologies

Source	Year	Focus of Study	Type of Materials Tested	Apparatus Used	Insights
[31]	1976	Qualitative erosion resistance	Dispersive clays	PET	Assessed erosion susceptibility in dispersive clays
[32]	1991	Erodibility related to soil tensile strength	Soils	Custom Test	Tied erodibility to soil's tensile strength
[33]	1991	Jet erosion test development	Soils	JET	Pioneered the use of jets to simulate natural erosion
[34]	1994	Long-term performance of cutoff barriers	Cement-bentonite	Laboratory Tests	Evaluated the longevity and effectiveness of barriers
[35]	2004	Erosion under dynamic water jets	Soils	JET	Focused on the impact of dynamic water jets on soils
[36]	2004	Quantifying erosion rates and triggers	Soils	HET	Developed quantifiable metrics for erosion rates
[37]	2006	Internal erosion mechanics in soils	Soils	PET with Resistivity Sensors	Studied mechanisms initiating internal erosion
[38]	2008	Erodibility classification based on hydraulic shear stress and velocity	Soils	EFA and other custom apparatus	Provides erodibility ranges for various soil types (untreated silt, clay, etc.).
[39]	2011	Comparative study of erosion tests	Soils	JET and HET	Compared different testing methods and their findings
[40]	2012	Internal and overtopping erosion processes affecting earth dams and landslide dams under complex stress states	Soils	Custom-designed stress-controlled erosion apparatus	Increased erosion risks with varying stress and loading conditions
[41]	2012	Critical hydraulic shear stress for untreated silt	Soils	HET	Proposed a higher range (400-500 Pa) compared to Briaud [32]
[42]	2017	Erosion resistance of lime-treated soils for coastal dikes	Soils	Multiple Tests (Mobile Jet Erosion Test (MoJET), HET, and Enhanced Crumb Test (ECT))	Lime-treated soils demonstrate substantially enhanced resistance to erosion compared to untreated soils, suggesting their potential efficacy in coastal dike construction
[43]	2013	Real-time erosion monitoring	Soils	HET	Implemented turbidity meters for real-time erosion tracking
[44]	2015	Modification of erosion tests	Soils	Modified HET	Proposed changes in the calculation of inlet head loss to improve test accuracy
[45]	2016	Hydraulic shear stress on erodibility	Treated soils	HET	Linked shear stress with erosion rate
[46]	2017	Hydraulic shear stress on erodibility	Soils	Modified HET	Improvements to the calculation or assessment of the head loss across the specimen's aperture.

These studies, ranging from the qualitative assessment of erosion susceptibility in dispersive clays [31] to the more recent investigations into the hydraulic shear stress on erodibility [46], highlight diverse methodologies and findings across decades. Traditional erosion testing methods, including the Hole Erosion Test (HET), Jet Erosion Test (JET), Erosion Function Apparatus (EFA) and Pinhole Erosion Test (PET), have been employed to evaluate the erosion resistance of soils and CB materials. However, these methods are typically conducted without the application of confining pressure, which limits their ability to replicate in-situ conditions accurately [36, 45-46]. While each study contributes valuable insights into specific aspects of soil behavior, a common limitation emerges: the applicability of these findings under complex loading conditions remains uncertain.

Complex loading conditions, comprising varying hydraulic pressures, mechanical stresses, and environmental factors, are essential to analyze because they more accurately reflect the real-world scenarios in which these materials must perform. However, current studies often rely on simplified laboratory or field setups [36, 41, 45] that fail to capture the full spectrum of interactions and rapid changes experienced in natural settings. This discrepancy between controlled experiments and actual operating environments introduces uncertainties in predicting erosion resistance and complicates the development of universally applicable design guidelines. Recognizing these challenges, the present study employs a modified triaxial testing apparatus capable of simulating both confining pressure and fluid flow concurrently, offering a more representative assessment of in-situ conditions. Such an advanced approach is crucial for devising effective, site-specific strategies that mitigate erosion risks and ensure the structural integrity of large-scale engineering projects.

An additional, closely related concern is the effect of curing period on the erodibility of cement-bentonite barriers. In practice, cement-bentonite barriers are subjected to mechanical stresses and hydraulic loading at different stages of their curing cycle; from immediately post-construction, during intermediate stages of curing, to well after full maturation. Each stage exhibits distinct physical and chemical characteristics due to the evolving matrix of the material, impacting the barrier's structural integrity and susceptibility to erosion. As detailed by Royal et al. [47], variations in environmental conditions such as drying and rewetting further influence these properties, emphasizing the need for comprehensive understanding of barrier behavior under realistic loading scenarios to ensure long-term effectiveness. Variations in barrier compositions, such as substituting portions of cement with GGBS or adjusting the bentonite content, add another layer of complexity, as these mixtures may respond differently to changes in loading over time [48]. Gaining a deeper understanding of how these factors intersect and evolve throughout the barrier’s service life is, therefore, a critical gap in knowledge.

To address these challenges, the present research aims to systematically investigate how complex loading conditions, varying curing periods, and different mix designs, including the use of various GGBS proportions, affect the erodibility behavior of cement-bentonite barriers. By integrating laboratory experiments with conditions more representative of field scenarios, this study endeavors to provide actionable insights that bridge the gap between controlled testing and real-world applications. The outcome will inform better design practices, particularly in selecting appropriate compositions, GGBS proportioning, and curing protocols, and offer engineers and decision-makers more reliable guidance on how to maintain the integrity and functionality of seepage barriers over their operational lifespan. Ultimately, these findings will contribute to safer, more resilient infrastructure, ensuring that dams, levees, and other critical systems remain effective under diverse and often unpredictable conditions.

2. Research Methodology

In line with the overarching goal of this research, namely, to elucidate how varying curing periods, mix compositions, and realistic loading conditions influence the erodibility of cement-bentonite barriers—a modified triaxial erosion testing approach was developed. As illustrated in Figure 1, which provides the overall research flow chart, this methodology directly addresses the need for more accurate simulations of practical scenarios by incorporating confining pressures into a triaxial setup specially adapted for erosion testing. By doing so, the investigation captures both erosive forces and confining stresses, reflecting the complex conditions these materials encounter in the field. This integrated design not only aligns with the study's aim to bridge laboratory findings with real-world applications but also provides a more appropriate framework for evaluating how curing duration and varying GGBS proportions affect the performance and stability of cement-bentonite mixtures against erosive force.

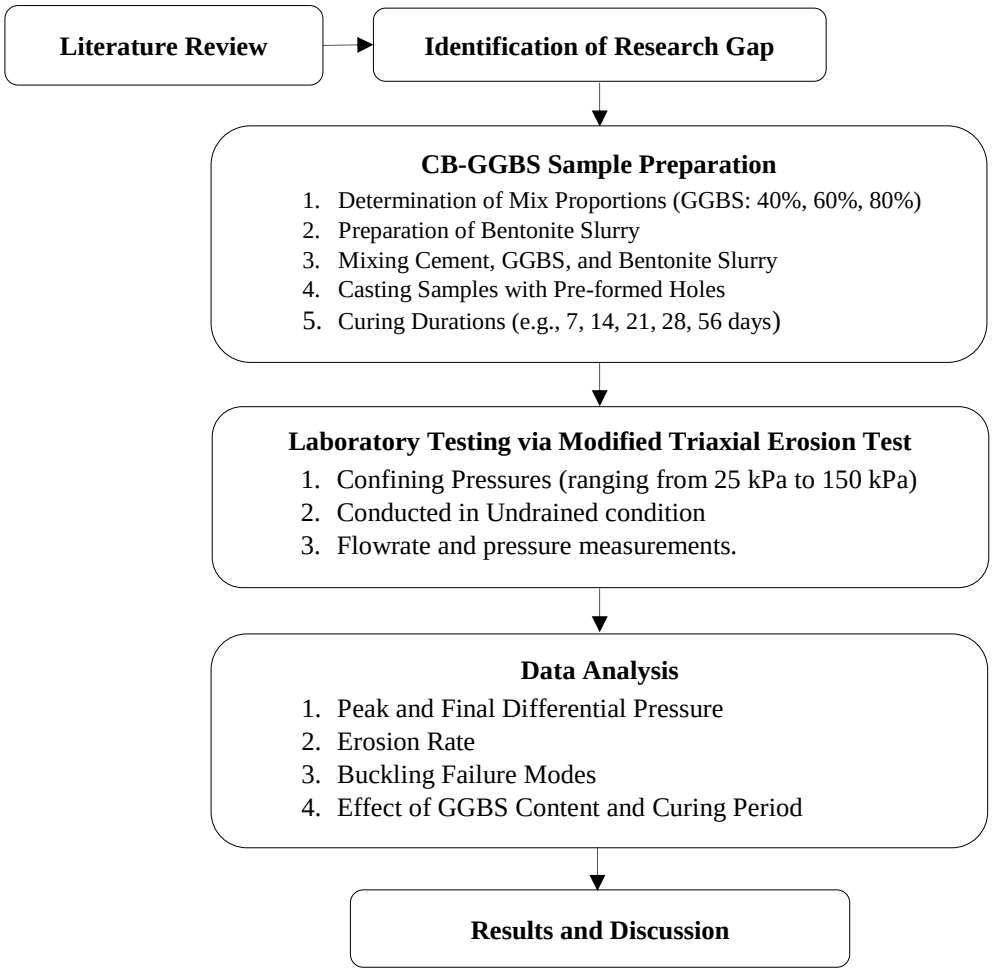

Figure 1. Research Flowchart

2.1. Samples Preparation

2.1.1. Samples Specification

The sample preparation process in this study follows the methodologies established by Royal et al. [47] and Walenna [49] for creating CB-GGBS mixtures. Three main materials were used: bentonite, cement, and ground granulated blast furnace slag (GGBS). For the bentonite component, Berkbent™ 163 was selected, a high-grade, free-flowing sodium

carbonate-activated bentonite. This bentonite is characterized by its fineness, with approximately 5% of the material retained on a 150-micron sieve after dry sieving, ensuring consistency and optimal mixing properties for use in cementitious blends [50]. The cement used in the mixture was Rugby® CEM II/B-V, a cement type that meets the requirements of British Standard EN 197-1: 2011. This cement contains a blend of 65–79% clinker, 21–35% siliceous fly ash, and up to 5% minor constituents [51]. The GGBS, sourced from Hansen Aggregates, has a typical chemical composition consisting of CaO (40%), SiO_2 (35%), Al_2O_3 (13%), and MgO (8%) [52].

2.1.2. Mixture Proportion

For the CB samples tested in the laboratory, four distinct mixture proportions were prepared, as shown in Table 2. Following the mix proportion established in the study by Royal et al. [52], the base mixture (CB without GGBS) consisted of 1000 mL of water, 200 g of cement, and 40 g of bentonite. This base mix served as a reference sample to evaluate the effect of GGBS replacement on sample behavior.

Table 2. Mixture Proportion

No	Sample Type	GGBS Replacement (%)	Sample Composition			
			Water (mL)	Bentonite (gr)	Cement (gr)	GGBS (gr)
1	CB with GGBS	40	1000	40	120	80
2	CB with GGBS	60	1000	40	80	120
3	CB with GGBS	80	1000	40	40	160
4	CB without GGBS	0	1000	40	200	-

The CB samples with GGBS were prepared with three different replacement levels: 40%, 60%, and 80% of the cement content. The 40% GGBS replacement sample was prepared with 1000 mL of water, 40 g of bentonite, 120 g of cement, and 80 g of GGBS, representing a moderate level of substitution. The 60% replacement sample contained 1000 mL of water, 40 g of bentonite, 80 g of cement, and 120 g of GGBS, which allowed for analyzing the effect of higher GGBS content. Lastly, the 80% GGBS replacement (Type 3) was produced by mixing 1000 mL of water, 40 g of bentonite, 40 g of cement, and 160 g of GGBS to observe the influence of maximum GGBS content on erosion resistance and consolidation behavior. The choice of the 80% replacement level aligns with Jefferis' recommendations for optimizing GGBS replacement [48, 53].

2.1.3. Sample Creation

In this study, the procedure to produce CB-GGBS samples was adapted from previous studies [28, 47, 49]. The sample preparation involved a series of steps to ensure consistency and reliability in the sample structure. The samples were prepared in cylindrical molds with a diameter of 50 mm, a height of 100 mm, and a central hole of 3 mm in diameter to simulate erosion pathways. This central hole was created by placing a 3 mm diameter acrylic rod in the mold, allowing it to mimic a pre-formed crack or hole. Table 3 summarizes each key stage in the preparation of cement-bentonite samples, ensuring consistency and reliability for subsequent testing and analysis.

Table 3. Overview of Cement-Bentonite Mixture Preparation Steps

Step	Procedure	Key Details
Bentonite Slurry Preparation	1. Dry bentonite was mixed with water for 25 ± 3 minutes using a commercial food mixer under controlled speed. 2. Every 10 minutes, the mixer bowl walls were scraped to prevent buildup. 3. The slurry was then left to hydrate for 24 ± 1 hour at room temperature, with the bowl covered to avoid contamination.	- Mixer speed was kept constant. - Ensured thorough scraping to maintain uniform mixing. - Covered slurry to prevent external contaminants.
Cementitious Material Mixing	1. Cement and GGBS were sieved to remove clumps. 2. The sieved materials were combined with the hydrated bentonite slurry for 5–7 minutes.	- Sieving essential to ensure homogeneity. - Uniform mixing for improved material consistency.
Mold Filling	1. The CB slurry was poured into cylindrical molds. 2. An acrylic rod was placed at the center to form a 3 mm hole through the sample. 3. The molds were capped on both ends to secure the rod in place.	- Central hole maintained throughout curing. - Caps prevent displacement of the acrylic rod.
Air Removal and Curing	1. Molds were placed on a vibrating table for 10–15 minutes to release entrapped air. 2. Samples were cured at 5–7°C to simulate typical ground temperatures. 3. Curing durations were set at 7, 14, 21, 28, and 56 days, depending on experimental needs.	- Vibrating helps remove air voids, improving sample integrity. - Low curing temperature (5–7°C) mimics in-situ conditions.
Sample Extraction and Submerging	1. After curing, samples were extracted, and the acrylic rod was carefully removed. 2. Preliminary tests indicated that reinserting rods could cause edge cracks.	- Minimizing disturbance during rod removal and sample extraction is crucial to maintain sample integrity.

During curing, the samples were submerged in the same water used in the CB slurry preparation to maintain consistency in material exposure and avoid chemical disturbances (as seen in Figure 2). This submersion ensured that the samples underwent continuous hydration, which contributed to their strength and durability for the erosion tests.

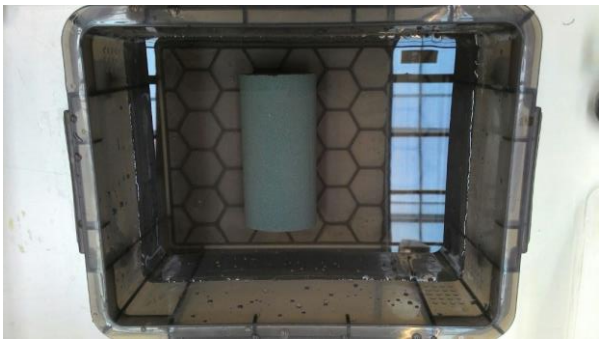

Figure 2. Sample Curing by Submersion

2.2. Testing Overview

The apparatus used in this study, termed the modified triaxial erosion test, was developed by adapting a traditional triaxial setup with custom modifications to enable erosion testing under controlled confining pressures (Figure 3).

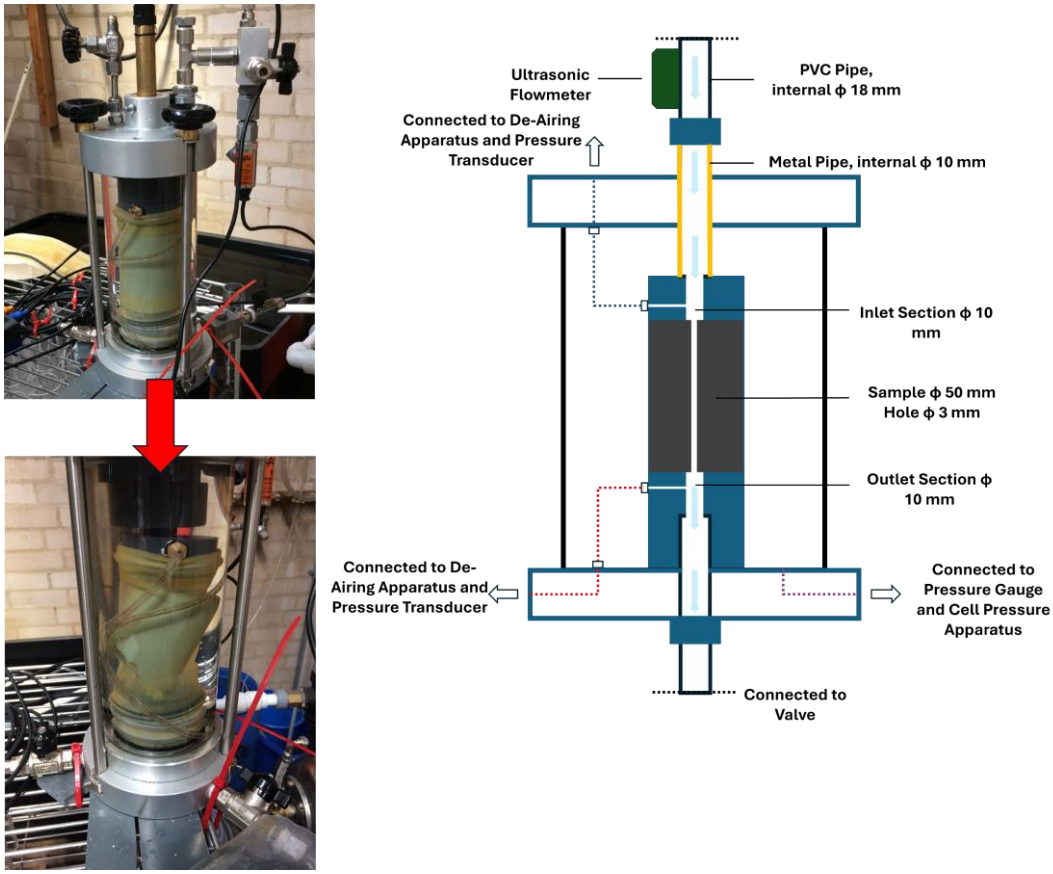

Figure 3. Testing Apparatus

These modifications were essential to allow for precise erosion testing within the framework of a triaxial apparatus, making it possible to simulate the combined effects of erosion and confinement. Unlike traditional erosion testing methods, such as HET and PET, which typically allow water to flow from an upstream to a downstream end through a sample constrained in a rigid tube, the modified triaxial erosion test applies confining pressures ranging from 25 to 150 kPa. Because standard HET or PET setups are limited by the rigid tube enclosure, they cannot accommodate varying external loading conditions that reflect field stresses. This range of pressures in the present apparatus allows for a detailed evaluation of how confining stress influences erosion resistance and structural stability in CB-GGBS samples. While previous studies have utilized modified triaxial setups to examine phenomena like particle migration and internal erosion [40, 54], they have not specifically addressed the erosion resistance of seepage barrier materials under variable confining pressures. By enabling simultaneous simulation of erosion and multiple stress states, this study advances the theoretical understanding of erosion processes under conditions that more closely mirror complex field environments, where

concurrent hydraulic and mechanical loads may alter erosion progression and potential failure modes. As a result, it fills an important gap by examining how increased confining pressures impact the erosion response and failure mechanisms of CB-GGBS samples, providing insights relevant to practical applications where materials face both erosive forces and confining stresses.

2.2.1. Technical Procedure

The modified triaxial erosion test used in this study builds upon the standard HET framework [36], incorporating significant modifications to enable controlled application of confining pressure, a feature not available in traditional HET and PET setups. The testing apparatus directs the eroding fluid vertically through the sample, with an entrance-to-initial hole diameter ratio of 3.3, as determined by the geometry of the triaxial cell provided by Controls Group (Figure 3). This setup facilitates a controlled erosion pathway through the sample while maintaining consistency in flow alignment and applied pressure.

To ensure a sealed testing environment, each sample was encased in a double-layered membrane, secured with rubber washers at both ends to prevent leakage. This sealing method, while effective, presented challenges during assembly, particularly for younger samples with shorter curing durations, which were prone to deformation or failure under handling. After assembly, the triaxial cell was clamped, and water was introduced into the central hole and pipework to expel any trapped air, followed by a thorough inspection to verify the absence of leaks and confirm proper test conditions.

Once the setup was validated, the triaxial cell was gradually filled with water, and confining pressure was applied incrementally, starting at 25 kPa and increasing up to a maximum of 150 kPa, depending on the specific requirements of each test. Due to the limitations of the testing apparatus, all samples were subjected to undrained conditions, which precluded any consolidation during the testing phase. This decision was made to avoid potential disturbances and structural changes that could occur under drained conditions, which might compromise the sample's integrity and influence test outcomes. Testing under undrained conditions ensured that the observed erosion behavior directly reflected the effects of the applied confining pressure without the confounding impact of consolidation processes.

Erosion testing continued for a specified duration (600 seconds) or until the onset of structural failure in the sample (as seen in Figure 4). Unlike traditional HET configurations, the erosion was not uniformly distributed along the length of the crack but tended to concentrate at the upper part of the sample, where the eroding fluid entered.

Figure 4. Typical Signs of the Onset of Sample Failure

2.2.2. Technical Consideration

The modified triaxial erosion test presented several technical challenges, particularly concerning the maintenance of confining pressure, regulation of flow conditions, and management of structural behavior under stress. These considerations were critical to ensuring the reliability and accuracy of the testing procedure.

2.2.2.1. Confining Pressure Stability

A primary technical issue was the difficulty in maintaining stable confining pressure throughout the test duration. Once particle detachment began, samples often exhibited cracking attributed to circumferential, or hoop stress, within the structure. These cracks created pathways that allowed the eroding fluid to interact with the confining fluid, destabilizing the applied confining pressure. Given that the pump pressure was generally higher than the confining pressure, this interaction led to the expansion of the membrane within the triaxial cell. As a result, the confining pressure within the cell equalized with the pump pressure, effectively negating the intended confining effect on the sample.

To address this issue, multiple pressure regulators were trialed in an attempt to stabilize cell pressure. However, the limitations inherent to the triaxial apparatus hindered the ability of the regulators to counteract rapid fluctuations effectively, particularly in the post-cracking phase. Venting excess pressure proved challenging, as the regulators were unable to respond swiftly enough to maintain the desired confining pressure. This limitation was especially pronounced at higher confining pressures, where maintaining stable pressure conditions was essential to ensure the validity of the results under varying structural states.

Although this study focused on static confining pressures, many field conditions are dynamic, especially near fault zones or where hydraulic fracturing operations occur [13]. Abrupt or repetitive changes in stress may widen micro-cracks or mobilize fine particles faster, potentially amplifying erosion. To capture these phenomena, future experimental protocols might include rapidly fluctuating or cyclic confining pressures to mimic seismic loading or fracturing events. A coupled mechanical-hydraulic model would further clarify how stress transients combine with ongoing erosion processes to affect the long-term stability of cement-bentonite barriers.

2.2.2.2. Flow and Pressure Regulation

Continuous monitoring of flow and pressure was essential throughout testing to capture accurate data on sample behavior under erosive forces. Unlike traditional HET setups, where testing typically proceeds uninterrupted for a fixed duration, the modified triaxial erosion test required termination of flow and pressure measurements upon detecting structural failure. This approach was necessary to prevent further structural degradation that could interfere with accurate analysis of erosion dynamics. Consequently, the test duration was often shorter than the standard 600 seconds, concluding as soon as indicators of failure, such as wall thinning or buckling, were observed

These technical considerations underscore the challenges of adapting traditional triaxial equipment for erosion testing under controlled confining pressures, emphasizing the importance of precise regulatory mechanisms and equipment capable of maintaining stable pressure conditions. The insights gained highlight the need for further refinement of equipment and testing protocols to accommodate the unique requirements of erosion testing under confined conditions.

2.2.2.3. Limitations Regarding Loading and Fluid Variations

The apparatus used in this study applies a static confining pressure to simulate in-situ overburden stresses. While this approach yielded valuable insights into the relationship between erosion mechanisms and confining pressures, it does not replicate cyclic loading (such as waves, seismic events, or repeated wet–dry cycles) or changes in fluid chemistry (e.g., salinity or pH). Adapting the current setup to accommodate fluctuating pressures or different fluid compositions would be a logical next step in capturing conditions closer to real-world scenarios. Future studies could integrate cyclic loading modules or test with fluids representing brackish or chemically aggressive environments to better understand the long-term durability of GGBS-containing CB barriers under varying stress states.

2.3. Parameters and Data Analysis

In this study, a comprehensive set of parameters was collected to assess the erosion resistance and structural responses of CB-GGBS samples under varying conditions. The primary data obtained from the modified triaxial erosion test included flow rate and pressure, recorded continuously via data loggers. Key parameters analyzed included peak differential pressure, final differential pressure, erosion deceleration points, and visual observations of failure mechanisms. The data analysis involved plotting pressure differential and flow rate against time to understand how these parameters evolved throughout the testing process, enabling the identification of critical points in sample behavior, such as the onset of erosion and structural instability.

Due to challenges in physically casting and measuring the eroded hole diameter (as seen in Figure 5), direct measurements of the eroded path were not feasible. Consequently, erosion resistance was inferred from the pressure and flow rate data. Some samples exhibited structural failure, manifesting as either shear or tension failures, which added complexity to data interpretation. This failure data provided valuable insights into the mechanical stability of the samples under confining pressure, highlighting specific failure modes linked to circumferential stress and sample composition.

Figure 5. Typical Form of Samples After Removal from Testing Apparatus

These analyses facilitated a deeper understanding of the failure mechanisms under erosive forces, which will be further discussed in subsequent sections.

3. Results and Discussion

3.1. Erosion Testing Parameters and Overview

In this study, a range of parameters were selected and controlled to evaluate the erosion resistance and failure mechanisms of CB-GGBS samples. Each parameter has a role in influencing the structural integrity of the samples and their ability to withstand erosive forces under varying conditions. These parameters, GGBS content, curing duration, confining pressure, peak and final differential pressures, erosion deceleration point, and visual observations, serve as key indicators of the material's performance and durability.

Table 4 provides an overview of each parameter, including a brief description, its expected correlation with erosion behavior, and how it will be interpreted in the context of this study. By examining these variables in detail, we aim to understand how material composition and environmental stresses shape the erosion resistance and failure patterns of CB-GGBS mixtures. This structured approach allows us to isolate the effects of each parameter and draw conclusions about the sample's response to erosion.

Table 4. Overview of Parameters, Correlations with Erosion Behavior, and Their Interpretations

Parameter	Description	Correlation with Erosion	Interpretation
GGBS Content (%)	Percentage of Ground Granulated Blast Furnace Slag in the sample	Higher GGBS content improves matrix density and erosion resistance	Determines erosion resistance; higher content expected to reduce erosion rates
Curing Duration (Days)	Time allowed for samples to cure before testing	Longer curing increases sample strength and cohesion	Extended curing durations lead to improved structural integrity, reducing erosion susceptibility
Confining Pressure (kPa)	External pressure applied to the sample during testing	Higher confining pressures restrict particle detachment, lowering erosion rate	Evaluates material stability under varied pressure conditions, indicating material's resilience
Peak Differential Pressure (kPa)	Maximum pressure difference before erosion onset	Reflects initial resistance to erosion initiation	Used to assess the threshold at which erosion begins, indicating sample strength
Final Differential Pressure (kPa)	Pressure difference at the end of the test	Indicates residual strength after erosion	Measures sample's resistance post-erosion, showing the extent of degradation over time
Erosion Deceleration Point	Time at which the erosion rate slows down significantly	Shows how quickly the sample stabilizes during erosion	Analyzes erosion progression and stability over time
Visual Observations (Cracks)	Visible structural changes post-testing	Indicates structural breakdown due to erosion and pressure	Correlates with observed pressure data, validating failure mechanisms

These parameters are essential for understanding the erosion resistance of CB-GGBS samples under different conditions, helping to determine how material composition and external stresses influence structural stability. The GGBS content is particularly significant as it modifies the sample's microstructure [55, 56], creating a denser matrix that inherently resists particle detachment during erosion. This effect is anticipated to become more pronounced with higher GGBS content [55], providing insight into optimal material formulations for erosion-resistant applications. Similarly, the curing duration plays a pivotal role in defining the sample's strength [55], as extended curing allows for more complete pozzolanic reactions between the cement and GGBS, leading to enhanced cohesion and resilience against erosive forces.

Additionally, confining pressure is a critical variable as it simulates the conditions under which these materials might operate in field applications. Higher confining pressures are expected to mitigate the onset and progression of erosion by restricting particle movement and reinforcing structural integrity. By analyzing the peak and final differential pressures, we can determine both the initial resistance of the samples to erosion and the state of the strength after significant material loss. This data, combined with observations of erosion deceleration points and visual evidence of structural failure, allows us to comprehensively assess the failure mechanisms and durability of the samples.

3.2. Effect of Confining Pressure and Curing Duration on Erosion Resistance

The typical erosion test results presented in Figure 6 demonstrate the effects of curing duration and confining pressure on the erosion resistance of the tested samples. CB with 40% GGBS was chosen for its representativeness across other tests, providing typical results that are replicated in other GGBS percentage configurations. Each sample configuration was tested at least 2-3 times to ensure reliability and reproducibility. The erosion test results presented in Figure 6 demonstrate the effects of curing duration and confining pressure on the erosion resistance of the samples. Across all samples, the initial peak pressure at the inlet (P-in) is followed by a gradual decline, marking the onset and progression of erosion. The pressure at the outlet (P-out) increases as the erosion process creates a larger flow path within the sample. According to Bernoulli's equation, an increase in the cross-sectional area of the flow (due to erosion enlarging the hole) leads to a corresponding increase in static pressure, resulting in the observed rise in P-out.

For samples cured for 21 and 28 days, the peak inlet pressure consistently remains at approximately 250 kPa, regardless of an increase in confining pressure from 25 to 50 kPa. This consistency indicates that by 21 days, the sample structure has gained sufficient strength to withstand changes in confining pressure without affecting the peak inlet pressure. However, an increase in curing duration from 21 to 28 days is associated with a higher final differential pressure (ΔP), which correlates with a smaller final hole diameter and therefore reduced erosion. This relationship confirms that longer curing time enhances the structural matrix of the sample, increasing its resistance to erosive forces. Additionally, an increase in confining pressure from 25 to 50 kPa further raises the final differential pressure, underscoring that both curing duration and confining pressure are factors in enhancing erosion resistance. With a further extended curing duration of 56 days, both the peak inlet pressure and final differential pressure increase. While the peak inlet pressure remains unchanged with an increase in confining pressure from 25 to 50 kPa, the final differential pressure continues to rise. This finding indicates that while the sample's resistance to peak pressure stabilizes after prolonged curing, its resistance to ongoing erosion continues to improve with higher confining pressure.

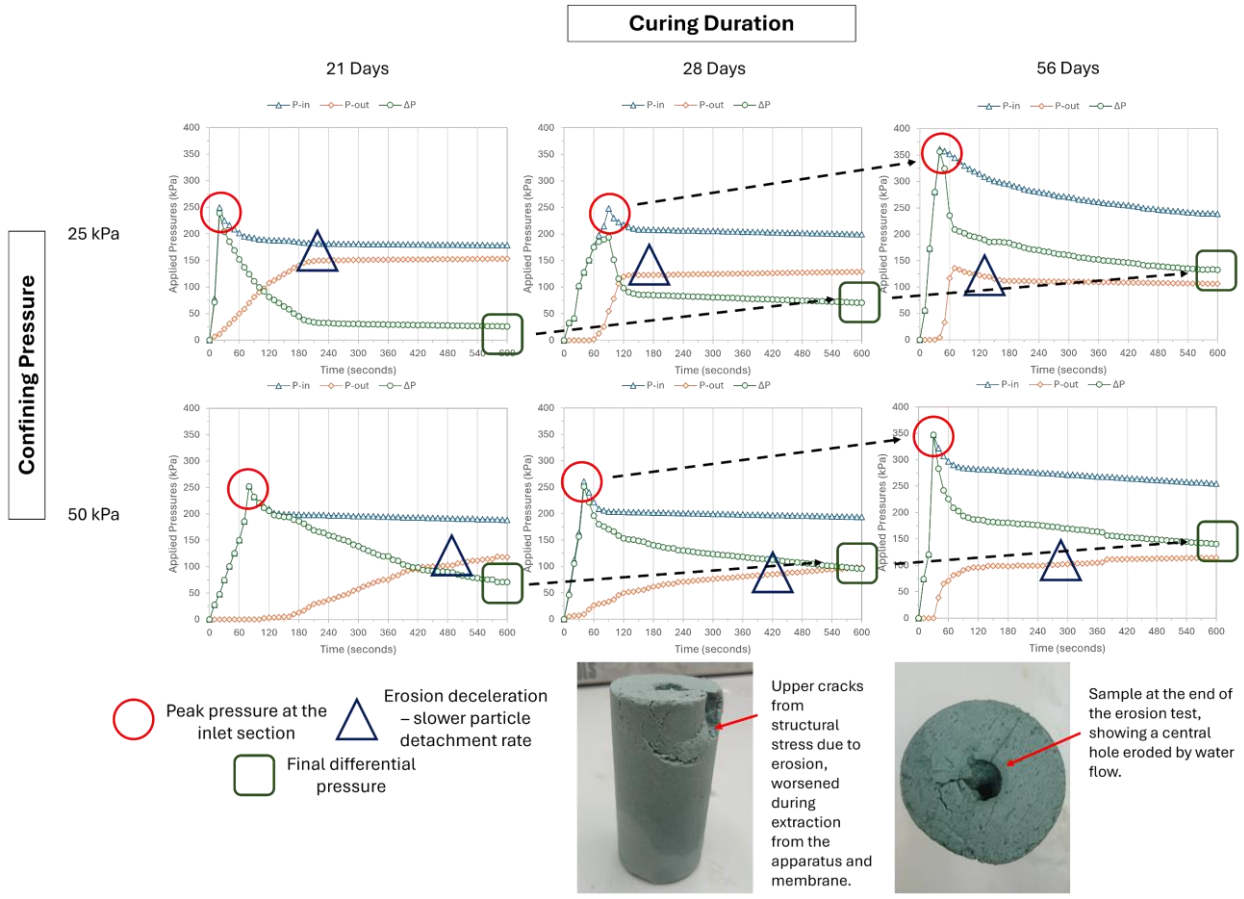

Figure 6. Representative Pressure-Time Responses in Erosion Testing: CB-GGBS 40% Samples Under Different Confining Pressures (25 and 50 kPa) and Curing Durations

The phase of erosion deceleration occurs later at a confining pressure of 50 kPa, indicating a slower rate of particle detachment. Conversely, at 25 kPa, erosion deceleration begins earlier, confirming that higher confining pressures contribute to structural improvement by slowing the rate of erosion. This delayed erosion phase indicates the role of confining pressure in reinforcing the sample's integrity, which reduces the rate at which particles detach.

Visible cracking on the upper sections of the samples is attributed to structural degradation caused by erosive forces, exacerbated by the extraction process from the apparatus and removal from the membrane (Figure 6). This interaction between erosion and mechanical stress weakens the sample structure, making it more susceptible to cracking under applied pressures. These cracks illustrate the cumulative impact of erosion and mechanical stress on the sample's structural stability, particularly in areas exposed to erosive flows and extraction forces.

With the introduction of a higher confining pressure of 100 kPa (as seen in Figure 7), the sample behavior exhibits distinct changes that highlight both enhanced erosion resistance and structural limitations. At this increased confining pressure, the peak inlet pressure increases across curing durations, with a progressive rise from 21 days to 28 and 56 days, signaling the material's increased threshold to erosion initiation. This trend aligns with observations at lower confining pressures, where extended curing strengthens the sample's structure. Additionally, the final differential pressure at 100 kPa surpasses the values recorded at 50 kPa for each respective curing period, reinforcing the correlation between higher confining pressures, longer curing durations, and reduced erosion rates. The higher final differential pressure indicates that the material maintains a smaller erosion-induced diameter by the end of the test, showing less material loss due to erosion.

However, a notable phenomenon observed at 100 kPa is the onset of early-stage buckling failure in the samples. This buckling failure occurs soon after the peak inlet pressure is reached, marked by a rapid drop in pressure, indicating structural collapse. Figure 7 shows that the samples lose part of their lower structure due to erosion, further weakening their resistance to axial stress. While similar buckling behavior is observed at 25 and 50 kPa, the effect is significantly more pronounced at 100 kPa. This suggests a trade-off between increased erosion resistance and the structural stability of the sample under higher confining pressures; while the samples exhibit improved resistance to erosion, they also become more vulnerable to mechanical instability when subjected to sustained axial stress and erosive forces. The early onset of buckling at 100 kPa highlights that there is a threshold pressure at which confining stress may compromise structural integrity, particularly in materials undergoing simultaneous erosion. This pattern emphasizes that while higher confining pressures generally improve erosion resistance by increasing peak and final differential pressures, they may also exacerbate mechanical weaknesses under certain conditions. Specifically, the combination of erosive forces and high confining stress introduces additional strain on the sample, potentially overwhelming the structural support of the material. This indicates that there is a balancing point between confining pressure and sample stability; beyond this threshold, the benefits of increased erosion resistance may be offset by the risk of structural collapse.

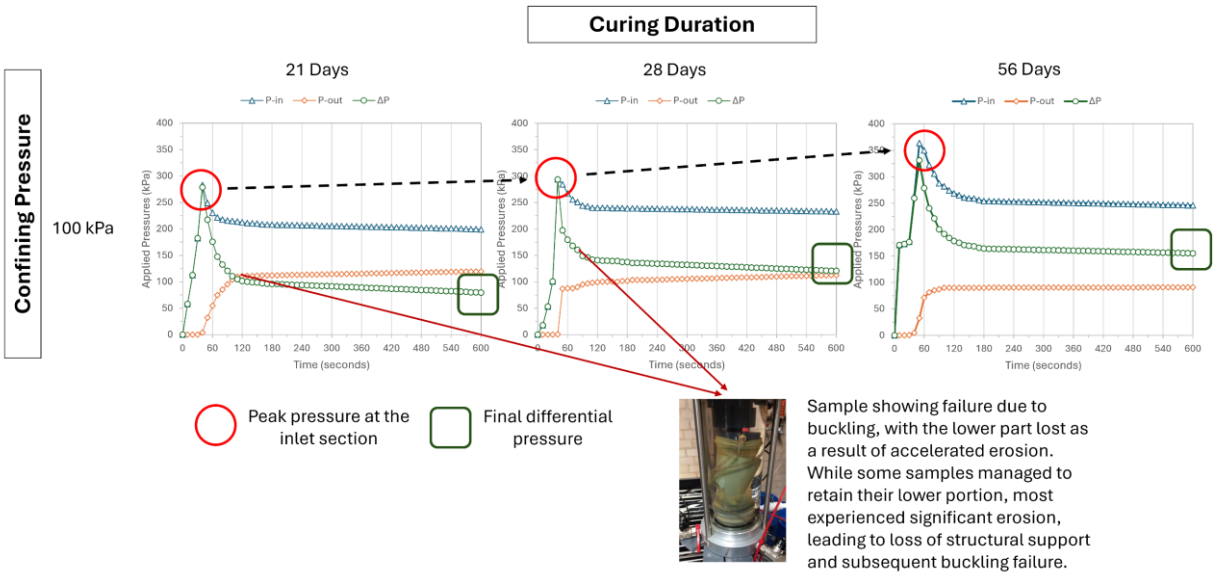

Figure 7. Representative Pressure-Time Responses in Erosion Testing: CB-GGBS 40% Samples Under 100 kPa Confining Pressure and Varying Curing Durations

As indicated in Figure 8, the results for the samples cured for 56 days under a confining pressure of 150 kPa reveal a distinct phenomenon of delayed erosion. Compared to the results from tests at 25, 50, and 100 kPa, the 150 kPa test demonstrates a more prolonged period of stability, with the inlet pressure (P-in) slowly decreasing and the outlet pressure (P-out) gradually increasing. This steady trend indicates that erosion is occurring at a slower rate, maintaining structural integrity for a longer duration before a significant change in pressure behavior occurs. The increase in both peak inlet pressure and final differential pressure suggests enhanced erosion resistance, further indicating that higher confining pressures contribute positively to structural stability against erosion.

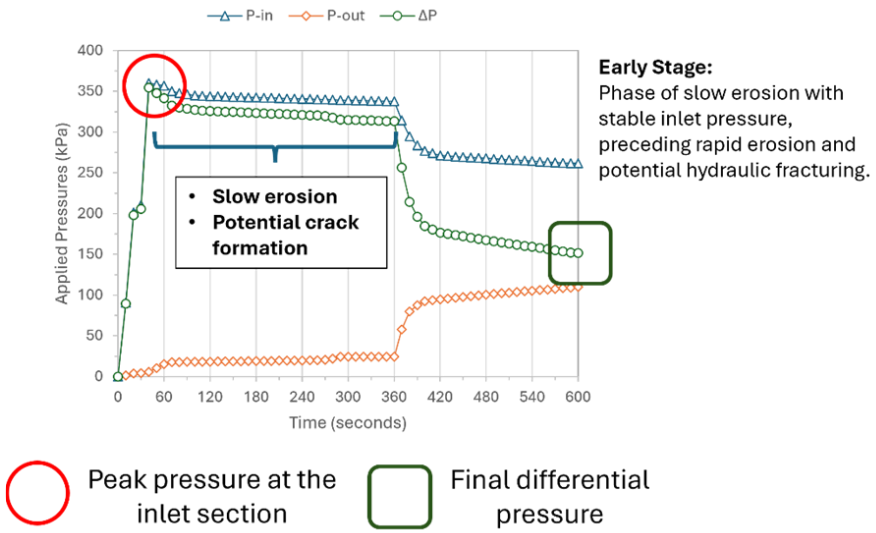

Figure 8. Representative Pressure-Time Responses in Erosion Testing: CB-GGBS 40% - 56 Days Curing Samples Under 150 kPa Confining Pressure

This delayed erosion phase, marked by a gradual decrease in inlet pressure (P-in) and a slow increase in outlet pressure (P-out), suggests the onset of microcrack development that can ultimately lead to hydraulic fracturing. Prolonged curing appears to strengthen the internal matrix, enabling the sample to better withstand high confining pressures during the early stages of erosion. However, over extended periods and particularly at elevated confining pressures (as seen in Figure 8), localized stress concentrations can form near partially hydrated clinker grains or bentonite layers. Once these microcracks coalesce, the erosion process may transition from a relatively slow progression to a more pronounced phase. In effect, curing delays the initial erosion but may shift the failure mode toward gradual crack propagation, culminating in hydraulic fracturing if pore pressures rise in these cracks. While increased confining pressure offers greater resistance to erosion by improving structural stability, it may also accelerate crack initiation under sustained loads, emphasizing the importance of optimizing confining pressures for long-term performance. This nuanced interplay between enhanced erosion resistance and potential internal fracturing underscores the need for continuous monitoring and strategic design considerations in barrier applications that demand both stability and durability.

3.3. Analysis of Peak and Final Differential Pressure

The results of the erosion testing for CB-GGBS samples with varying GGBS contents (40%, 60%, and 80%) and different curing durations, as seen in Figures 9 and 10, provide insights into the materials' erosion resistance at both the onset of erosion (peak differential pressure) and at the stabilized end point (final differential pressure). Higher peak and final differential pressures signify better resistance to erosion, reflecting both initial resistance and the ability to retain structural integrity.

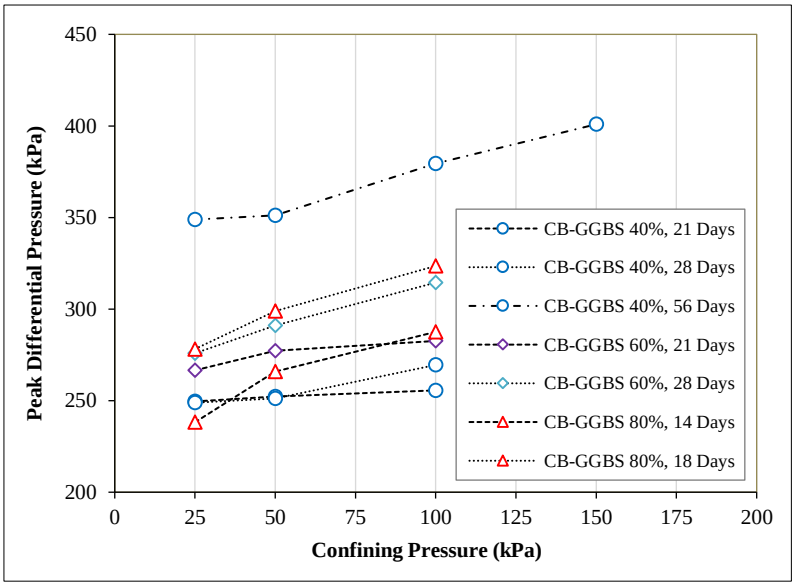

Figure 9. Peak Differential Pressure of CB-GGBS Samples Under Different GGBS Contents, Curing Durations, and Confining Pressures

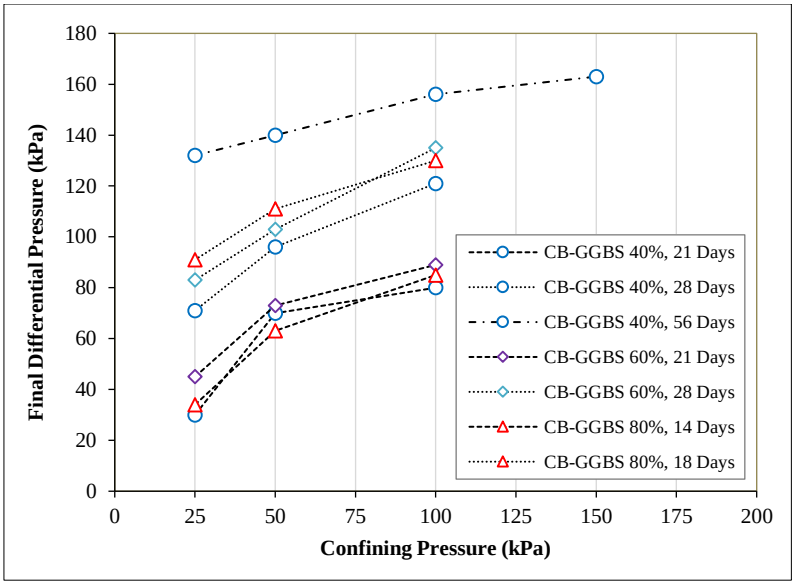

Figure 10. Final Differential Pressure of CB-GGBS Samples Under Different GGBS Contents, Curing Durations, and Confining Pressures

3.3.1. Influence of Confining Pressure on Peak and Final Differential Pressure

For all CB-GGBS compositions and curing durations, both peak and final differential pressures consistently increase with confining pressure, indicating that higher confining pressures enhance structural integrity. For example, CB-GGBS 40% samples cured for 56 days reached peak differential pressures of approximately 400 kPa and final differential pressures of around 160 kPa at a confining pressure of 150 kPa, compared to around 250 kPa (peak) and 60 kPa (final) at a confining pressure of 25 kPa. This represents a 60% increase in peak differential pressure and a 167% increase in final differential pressure as confining pressure rises, underscoring the importance of stress state in delaying erosion onset and minimizing material loss.

The CB-GGBS 40% samples exhibit consistent increases in both peak and final differential pressures, with estimated increases of 20-30% with each increment in confining pressure. For instance, at 56 days of curing, peak differential pressure increases from approximately 300 kPa at 50 kPa confining pressure to nearly 350 kPa at 100 kPa, while final differential pressure rises from around 100 kPa to 140 kPa under the same conditions. This pattern suggests that higher confining pressures limit particle detachment and erosion progression by reinforcing the sample's matrix, thereby delaying erosion onset and reducing the extent of erosion.

3.3.2. Effect of GGBS Content and Curing Duration on Erosion Resistance

Peak and final differential pressures increase significantly with both curing duration and confining pressure. For example, at a confining pressure of 100 kPa, peak differential pressure for CB-GGBS 40% increases from approximately 280 kPa at 21 days to nearly 350 kPa at 56 days, a rise of about 25%. Similarly, final differential pressure increases from about 80 kPa to nearly 140 kPa under the same conditions, reflecting a 75% improvement. These trends indicate that prolonged curing enhances the matrix's cohesion through ongoing pozzolanic reactions [42, 50], creating a more cohesive and erosion-resistant structure.

In contrast, samples with higher GGBS contents (60% and 80%) demonstrate such high structural strength at longer curing durations that observable erosion behavior is limited. CB-GGBS 60% samples were not tested at 56 days due to their high strength, which prevented measurable erosion under standard testing conditions. Similarly, CB-GGBS 80% samples were only tested up to 18 days, as samples cured for 21 days or more displayed peak and final differential pressures beyond the capacity of the current testing equipment, making erosion testing impractical. For example, CB-GGBS 80% samples at 18 days reached peak differential pressures of approximately 300 kPa and final differential pressures of around 120 kPa at a 50 kPa confining pressure. This suggests that higher GGBS content strengthens the matrix substantially, preventing erosion even at elevated pressures and shorter curing times.

While the results in this study demonstrated that higher GGBS contents (up to 80%) markedly enhance the erosion resistance of cement-bentonite barriers, practical implementation must consider both the cost of GGBS and potential constructability issues. Typically, GGBS is less expensive than ordinary Portland cement per unit mass, but extremely high replacement levels can influence workability, setting time, and availability, which in turn can affect project

scheduling and economics. Although our testing did not explicitly quantify cost–benefit ratios, prior studies (e.g., [48]) suggest that 60–70% replacement often provides an optimal balance between performance and cost. Beyond this range, minimal further gains in erosion resistance may not justify the additional complexities introduced. Future work could examine a comprehensive life-cycle cost analysis, including transport and handling costs, to determine an upper threshold that balances both performance and economic viability.

3.3.3. Combined Observations and Implications

The combined data for peak and final differential pressures reveal that GGBS content, curing duration, and confining pressure all significantly impact erosion resistance. CB-GGBS 40% samples demonstrate a consistent increase in both peak and final differential pressures across a range of conditions, making them a good reference for measurable erosion resistance under standard testing. However, samples with higher GGBS content (60% and 80%) show even greater improvements, especially under longer curing durations and higher confining pressures, suggesting that they could provide enhanced erosion resistance and structural stability beyond the capabilities observed in 40% GGBS samples.

These findings open new opportunities for further investigation, particularly with high-capacity testing equipment that can accommodate the increased strength of CB-GGBS 60% and 80% samples at extended curing durations. Testing these higher-GGBS samples under advanced conditions could provide further insights into their erosion resistance and structural stability under extreme confining pressures, as conventional testing equipment may not fully capture their upper limits of performance.

Overall, the results underscore the importance of adjusting GGBS content, curing duration, and confining pressure to maximize erosion resistance. This combination of factors is particularly relevant for applications demanding durable, erosion-resistant materials, where high-GGBS mixtures may offer superior performance. Future studies with tailored testing approaches may be necessary to accurately assess the erosion resistance and mechanical stability of these high-strength samples under extreme conditions.

3.4. Buckling and Localized Failure Mechanism

The progressive erosion and subsequent buckling failure observed in erosion testing of CB-GGBS samples follow a distinct sequence of mechanical and structural changes. As illustrated in Figure 11, this sequence begins with initial material erosion, progresses through wall thinning and stress accumulation, and culminates in structural collapse. Understanding each stage of this mechanism provides insights into the erosion resistance and failure behaviors of materials under confining pressures. Table 5 outlines the key stages of the buckling and localized failure mechanism during erosion testing, illustrating the combined effects of internal fluid pressure, material erosion, and circumferential stress concentration.

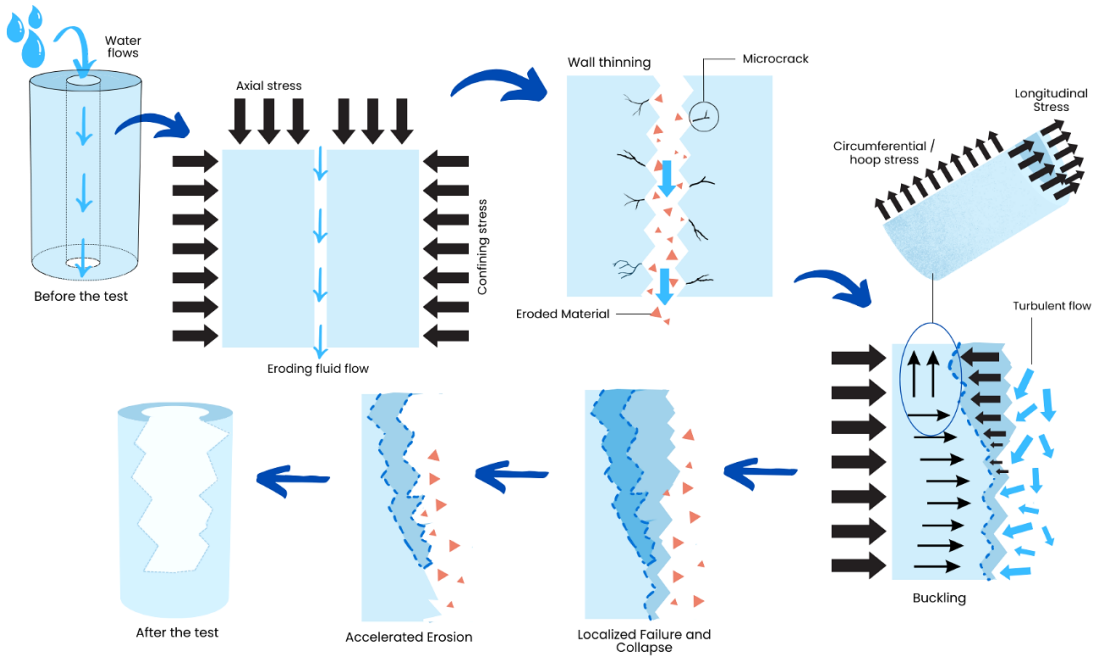

Figure 11. Illustrated Mechanism of Buckling and Localized Failure During Erosion Testing of Cement-Bentonite Samples

Table 5. Stages of Buckling and Localized Failure Mechanism in Erosion Testing

Stage	Description
Initial Erosion Phase	Fluid flow initiates material removal from the inner surface of the pre-formed hole, focusing on weak points like micro-cracks or irregularities in the soil matrix, where stress concentrations make the structure more susceptible to erosion.
Wall Thinning	As erosion progresses, material is lost from the inner walls, reducing the cross-sectional area resisting applied forces. This thinning raises internal stresses within the remaining soil structure, heightening its vulnerability to external pressure.
Circumferential (Hoop) Stress Accumulation	Circumferential (hoop) stress acts within the cylindrical sample to counteract the outward pressure exerted by the eroding fluid. As wall thickness decreases, hoop stress becomes increasingly concentrated, especially around weakened sections.
Approaching Critical Buckling Stress	Continued wall thinning leads to increased localized stress, eventually reaching a critical buckling stress threshold. At this point, the material is unable to maintain its shape and stability under the combined forces of erosion and external load.
Buckling Initiation	When critical buckling stress is exceeded, the sample wall buckles, either collapsing inward or bulging outward. This buckling results from the interaction of concentrated hoop stress and fluid pressure, leading to localized structural instability.
Localized Failure and Collapse	Buckling initiates a localized failure, causing parts of the soil structure to collapse into the eroded hole. This sudden failure occurs as the weakened area can no longer support the applied forces, leading to a structural breakdown.
Accelerated Erosion	The collapsed particles, now detached from the cohesive soil matrix, are more susceptible to fluid flow, resulting in accelerated erosion. The erosion rate increases as loose particles are carried away, further compromising the sample's integrity.

The failure mechanism observed in the CB-GGBS samples during erosion testing highlights a complex interaction between erosion processes and mechanical stress responses. As the inner walls erode, circumferential stress accumulates within the sample structure, ultimately reaching a critical point where the weakened walls can no longer resist the combined forces of hoop stress and fluid flow. This accumulation leads to buckling, where structural instability manifests as wall collapse or outward bulging. This sequence, from initial erosion to accelerated breakdown, demonstrates the sample's progressive weakening under sustained erosive forces and axial pressure.

The present study suggested that although higher confining pressures (>100 kPa) improve initial erosion resistance, they can also induce buckling failures when the sample's internal matrix erodes or micro-cracks accumulate. This suggests that there is a potential "threshold" pressure beyond which further increases in confinement may exacerbate structural instability. For applications such as deep-water environments or heavily loaded foundations, engineers must balance the benefit of enhanced erosion resistance against the increased risk of mechanical failure. In practice, this balance will hinge on site-specific subsurface conditions, for example, if overburden or hydrostatic pressures exceed 100–150 kPa, it may be necessary to adjust the mix design (e.g., higher bentonite content or different additives) or incorporate reinforcing elements to mitigate buckling risk.

Understanding this failure mechanism is crucial for designing erosion-resistant materials in civil engineering applications. The findings underscore the importance of evaluating both material composition and stress conditions in real-world scenarios, as increased confining pressures and curing durations enhance resistance to initial erosion but also introduce susceptibility to mechanical failure if critical stress thresholds are exceeded. Future applications must consider these trade-offs, particularly in environments where materials are subject to prolonged stress and fluid flow, ensuring that material selection and structural design accommodate the risks of localized failure and rapid erosion progression.

3.5. Summary and Design Implications

To conclude this section, we summarize the key findings from the erosion tests and outline the practical implications for design and engineering applications. The results highlight the influence of critical parameters, such as GGBS content, curing duration, and confining pressure, on the erosion resistance and mechanical stability of CB-GGBS samples. Table 6 lists the primary findings and their design implications, providing guidance for selecting optimal material formulations and conditions to maximize erosion resistance in practical, site-related applications.

Table 6. Primary Findings and Design Implications for Optimizing Erosion Resistance

Findings	Design Implications
Increased GGBS content (60% and 80%) significantly enhances erosion resistance, particularly at higher curing durations.	Using higher GGBS content in mix designs can provide increased durability and erosion resistance, especially suitable for structures exposed to aggressive environmental conditions.
Longer curing durations lead to improved structural cohesion, as indicated by higher final differential pressures.	Extended curing times should be considered where feasible, particularly for applications requiring enhanced long-term erosion resistance, such as groundwater barriers or embankments.
Higher confining pressures improve both peak and final differential pressures, demonstrating enhanced resistance to erosion.	Implementing controlled confining pressures or preloading techniques can enhance material stability and resistance to erosion in situ, supporting better performance under load-bearing conditions.
Buckling failure occurs at elevated confining pressures (100 kPa and above), indicating a trade-off between erosion resistance and structural stability.	Design considerations should account for the potential for buckling under high-stress conditions; materials should be tested to ensure they can withstand both erosion and mechanical stress without compromising stability.
The delayed erosion phase observed at higher confining pressures and longer curing durations suggests gradual crack formation leading to potential hydraulic fracturing.	Structural designs should consider stress thresholds to prevent hydraulic fracturing, particularly in applications where sustained stress and erosive forces coexist, such as cutoff walls or erosion-prone slopes.

These findings emphasize the complex relationship between material composition, curing, and environmental stresses, highlighting the need for balanced design approaches that optimize erosion resistance without compromising structural stability. Future research should focus on exploring the behavior of high-GGBS samples (60% and 80%) under increased confining pressures, which current testing equipment may not fully accommodate. Investigating these materials under extreme conditions can provide a deeper understanding of their upper limits of performance, informing advanced material formulations for durable, erosion-resistant engineering solutions.

4. Conclusions

In the comprehensive analysis of cement-bentonite barriers' erosion resistance, this research has investigated the effects of GGBS content, confining pressures, and curing periods. Here is a conclusion that highlights the critical findings from the study, focusing on the variables studied, their observed trends, the data-driven conclusions, and the technical limitations of the apparatus used:

- Increasing the GGBS content in CB barriers significantly enhances erosion resistance. The study quantitatively demonstrated that barriers with 40%, 60%, and 80% GGBS content exhibited progressively lower erosion rates, with the highest GGBS content showing up to a 50% reduction in erosion compared to the control samples without GGBS. This improvement is attributed to the denser and more cohesive microstructure facilitated by the pozzolanic reaction of GGBS.
- The erosion resistance of CB barriers improved with increasing confining pressures. However, at 100 kPa and above, although initial resistance to erosion was higher, there was a noted increase in the occurrence of buckling failures, indicating that while moderate increases in confining pressure enhance barrier integrity, excessive pressure can lead to structural vulnerabilities.
- The results revealed that longer curing periods correlated with significantly enhanced erosion resistance. Samples cured for 28 days showed a 40% improvement in erosion resistance over those cured for 7 days. This trend is linked to the continued hydration and strength development over time, emphasizing the importance of adequate curing in achieving optimal barrier performance.
- Higher confining pressures and extended curing periods were found to delay the onset of erosion, with the material exhibiting gradual crack formation over extended periods. This suggests a complex interaction between the material's time-dependent properties and the applied stresses, which could potentially lead to hydraulic fracturing under specific conditions.
- The modified triaxial erosion testing setup, while providing valuable insights, has limitations in simulating complex erosive forces and load conditions. The apparatus is primarily designed to apply uniform pressures and cannot fully replicate the dynamic and uneven stress distributions typically experienced in field environments. This limitation may affect the generalizability of the results to actual scenarios where barriers face irregular and fluctuating stresses.
- By integrating these quantitative findings, the study provides critical insights into the design and optimization of CB barriers. For instance, selecting a GGBS content of 60-80%, applying confining pressures around 50-75 kPa, and ensuring a minimum curing period of 28 days are recommended to optimize erosion resistance while minimizing the risk of mechanical failures such as buckling.

These conclusions emphasize the importance of a tailored approach to designing and implementing CB barriers, where the specific environmental and operational conditions are considered to maximize performance and longevity. This research significantly advances the understanding of how varying material compositions and operational conditions impact the erosion resistance of CB barriers, providing valuable guidance for future civil engineering applications

5. Declarations

5.1. Author Contributions

Conceptualization, M.A.W., A.R., I.J., and G.S.; methodology, M.A.W., A.R., I.J., and G.S.; software, M.A.W. and T.H.; validation, M.A.W. and A.R.; formal analysis, M.A.W., A.R., A.A., and Z.A.H.; investigation, M.A.W. and A.R.; resources, M.A.W., A.R., and T.H.; data curation, M.A.W., A.R., and Z.A.H.; writing—original draft preparation, M.A.W., A.R., I.J., and G.S.; writing—review and editing, M.A.W., A.A., and Z.A.H.; visualization, M.A.W. and Z.A.H.; supervision, M.A.W, A.R., I.J., G.S., and T.H.; project administration, M.A.W.; funding acquisition, M.A.W. All authors have read and agreed to the published version of the manuscript.

5.2. Data Availability Statement

The data presented in this study are available in the article.

5.3. Funding

This research was supported by the Lembaga Penelitian dan Pengabdian Masyarakat, Universitas Hasanuddin, under the funding scheme of Penelitian Fundamental Kolaboratif (Grant Number: 00309/UN4.22/PT.01.03/2024).

5.4. Acknowledgements

The authors extend their gratitude to the Lembaga Penelitian dan Pengabdian Masyarakat at Universitas Hasanuddin for their generous support and assistance in facilitating this research.

5.5. Conflicts of Interest

The authors declare no conflict of interest.

6. References

[1] Garvin, S. L., & Hayles, C. S. (1999). Chemical compatibility of cement-bentonite cut-off wall material. Construction and Building Materials, 13(6), 329–341. doi:10.1016/S0950-0618(99)00024-0.

[2] Flessati, L., Vecchia, G. Della, & Musso, G. (2023). Effects of curing on the hydro-mechanical behaviour of cement-bentonite mixtures for cut-off walls. Construction and Building Materials, 383. doi:10.1016/j.conbuildmat.2023.131392.

[3] Thapa, I., Kumar, N., Ghani, S., Kumar, S., & Gupta, M. (2024). Applications of bentonite in plastic concrete: a comprehensive study on enhancing workability and predicting compressive strength using hybridized AI models. Asian Journal of Civil Engineering, 25(4), 3113–3128. doi:10.1007/s42107-023-00966-x.

[4] Liu, M., Hu, Y., Lai, Z., Yan, T., He, X., Wu, J., Lu, Z., & Lv, S. (2020). Influence of various bentonites on the mechanical properties and impermeability of cement mortars. Construction and Building Materials, 241, 118015. doi:10.1016/j.conbuildmat.2020.118015.

[5] Waqas, R. M., Butt, F., Danish, A., Alqurashi, M., Mosaberpanah, M. A., Masood, B., & Hussein, E. E. (2021). Influence of bentonite on mechanical and durability properties of high-calcium fly ash geopolymer concrete with natural and recycled aggregates. Materials, 14(24), 7790. doi:10.3390/ma14247790.

[6] Fode, T. A., Jande, Y. A. C., & Kivevele, T. (2024). Effects of raw and different calcined bentonite on durability and mechanical properties of cement composite material. Case Studies in Construction Materials, 20, e03012. doi:10.1016/j.cscm.2024.e03012.

[7] Nugroho, S. A., Wardani, S. R., Muntohar, A. S., & Satibi, S. (2024). Effect of Coal Combustion Waste on Cement-Treated Clay. Civil Engineering Journal, 10(11), 3603-3612. doi:10.28991/CEJ-2024-010-11-010.

[8] Wei, J., & Gencturk, B. (2019). Hydration of ternary Portland cement blends containing metakaolin and sodium bentonite. Cement and Concrete Research, 123, 105772. doi:10.1016/j.cemconres.2019.05.017.

[9] Alaneme, G. U., & Mbadike, E. M. (2021). Optimisation of Strength Development of Bentonite and Palm Bunch Ash Concrete Using Fuzzy Logic. International Journal of Sustainable Engineering, 14(4), 835–851. doi:10.1080/19397038.2021.1929549.

[10] Lemonis, N., Tsakiridis, P. E., Katsiotis, N. S., Antiohos, S., Papageorgiou, D., Katsiotis, M. S., & Beazi-Katsioti, M. (2015). Hydration study of ternary blended cements containing ferronickel slag and natural pozzolan. Construction and Building Materials, 81, 130–139. doi:10.1016/j.conbuildmat.2015.02.046.

[11] Soga, K., Joshi, K., & Evans, J. C. (2013). Cement bentonite cutoff walls for polluted sites. Coupled phenomena in environmental geotechnics. Taylor Francis Group, London, United Kingdom. doi:10.1201/b15004-15.

[12] Musso, G., Vespo, V. S., Guida, G., & Della Vecchia, G. (2023). Hydro-mechanical behaviour of a cement–bentonite mixture along evaporation and water-uptake controlled paths. Geomechanics for Energy and the Environment, 33, 100413. doi:10.1016/j.gete.2022.100413.

[13] Rice, J. D., & Duncan, J. M. (2010). Deformation and Cracking of Seepage Barriers in Dams due to Changes in the Pore Pressure Regime. Journal of Geotechnical and Geoenvironmental Engineering, 136(1), 16–25. doi:10.1061/(asce)gt.1943-5606.0000241.

[14] Xu, B., Zou, D., Kong, X., Hu, Z., & Zhou, Y. (2015). Dynamic damage evaluation on the slabs of the concrete faced rockfill dam with the plastic-damage model. Computers and Geotechnics, 65, 258–265. doi:10.1016/j.compgeo.2015.01.003.

[15] Sun, W., Zhang, G., & Zhang, Z. (2021). Damage analysis of the cut-off wall in a landslide dam based on centrifuge and numerical modeling. Computers and Geotechnics, 130, 103936. doi:10.1016/j.compgeo.2020.103936.

[16] Wen, L., Cao, W., & Li, Y. (2023). Behavior of a Concrete-Face Rockfill Dam Cutoff Wall Considering the Foundation Seepage–Creep Coupling Effect. International Journal of Geomechanics, 23(5), 4023031. doi:10.1061/ijgnai.gmeng-8177.

[17] Cao, B., Chen, J., & Al-Tabbaa, A. (2021). Crack-resistant cement–bentonite cut-off wall materials incorporating superabsorbent polymers. Canadian Geotechnical Journal, 58(6), 800–810. doi:10.1139/cgj-2020-0181.

[18] Garner, S. J., & Fannin, R. J. (2010). Understanding internal erosion: a decade of research following a sinkhole event. The international journal on hydropower & dams, 17(3), 93.

[19] Chowdhury, K., Beswick, M., Waltz, J., Soga, K., Millet, R., Williams, T., & Orgill, S. (2020). Seepage cutoff walls: Lessons learned, implemented, and to be implemented. Association of State Dam Safety Officials Annual Conference, Dam Safety 21-25 September, 2020, Online.

[20] Zhang, Y., Cui, L., Jeng, D. S., Wang, Z., & Zhai, H. (2025). Erosion–Seepage System (ESS) for Flow-Induced Soil Erosion Rate with Seepage. Journal of Marine Science and Engineering, 13(1), 152. doi:10.3390/jmse13010152.

[21] Zhao, T., Wu, W., Fu, C., & Huo, D. (2024). Simulation of landslide dam failure due to overtopping considering vertical soil particles distribution. Geomatics, Natural Hazards and Risk, 15(1), 2366371. doi:10.1080/19475705.2024.2366371.

[22] Pereira, G. (2024). Cutoffs in dams: overview and recent developments. Geotechnical Engineering Challenges to Meet Current and Emerging Needs of Society, 187–196, CRC Press, Boca Raton, United States. doi:10.1201/9781003431749-13.

[23] Wang, J., Chai, J., Xu, Z., Geng, K., & Zhang, P. (2024). A review of barrier properties of polymer-modified bentonite applied to vertical cutoff walls under dry-wet cycling and chemical erosion. Journal of Water Process Engineering, 65, 105759. doi:10.1016/j.jwpe.2024.105759.

[24] Alrowais, R., Alwushayh, B., Bashir, M. T., Nasef, B. M., Ghazy, A., & Elkamhawy, E. (2023). Modeling and Analysis of Cutoff Wall Performance Beneath Water Structures by Feed-Forward Neural Network (FFNN). Water (Switzerland), 15(21), 3870. doi:10.3390/w15213870.

[25] Beier, H., & Strobl, T. (1985). Resistance against internal erosion of various types of cutoff walls in dam construction. Proceedings of the 15th ICOLD Congress, 24-28 June, 1985, Lausanne, Switzerland.

[26] Braithwaite, N. E. (2013). Laboratory modeling of erosion potential of seepage barrier material. Master Thesis, Utah State University, Logan, United States.

[27] Alonso, U., Missana, T., Fernández, A. M., & García-Gutiérrez, M. (2018). Erosion behaviour of raw bentonites under compacted and confined conditions: Relevance of smectite content and clay/water interactions. Applied Geochemistry, 94, 11–20. doi:10.1016/j.apgeochem.2018.04.012.

[28] Wang, Z., Zhao, B., & Royal, A. C. D. (2017). Investigation of Erosion of Cement-Bentonite via Piping. Advances in Materials Science and Engineering, 2017. doi:10.1155/2017/1762042.

[29] Garand, P., Bigras, A., Rattue, D. A., Hammamji, Y., & Saucet, J. P. (2006). Erosion resistance of plastic concrete. Transactions of the International Congress on Large Dams, 18-23 June, 2006, Barcelona, Spain.

[30] Walenna, M. A., Royal, A. C. D., Jefferson, I., & Ghataora, G. S. (2018). Investigating the erosion resistance of cement-bentonite barrier material using hole erosion test. Scour and Erosion IX, 31–32, CRC Press, Boca Raton, United States. doi:10.1201/9780429020940-6.

[31] Sherard, J. L., Dunnigan, L. P., & Decker, R. S. (1976). Identification and nature of dispersive soils. Journal of the Geotechnical Engineering Division, 102(4), 287-301. doi:10.1061/ajgeb6.0000256.

[32] Nearing, M. A., Simanton, J. R., Norton, L. D., Bulygin, S. J., & Stone, J. (1999). Soil erosion by surface water flow on a stony, semiarid hillslope. Earth Surface Processes and Landforms: The Journal of the British Geomorphological Research Group, 24(8), 677-686. doi:10.1002/(SICI)1096-9837(199908)24:8<677::AID-ESP981>3.0.CO;2-1.

[33] Hanson, G. J. (1990). Surface erodibility of earthen channels at high stresses. Part II - Developing an in situ testing device. Transactions of the American Society of Agricultural Engineers, 33(1), 132–137. doi:10.13031/2013.31306.

[34] Evans, J. (1994). Hydraulic Conductivity of Vertical Cutoff Walls. Hydraulic Conductivity and Waste Contaminant Transport in Soil, 79–94, The American Society of Mechanical Engineers, New York, United States. doi:10.1520/stp23885s.

[35] Hanson, G. J., & Cook, K. R. (2004). Apparatus, Test Procedures, and Analytical Methods to Measure Soil Erodibility in Situ. Applied Engineering in Agriculture, 20(4), 455–462. doi:10.13031/2013.16492.

[36] Wan, C. F., & Fell, R. (2004). Investigation of Rate of Erosion of Soils in Embankment Dams. Journal of Geotechnical and Geoenvironmental Engineering, 130(4), 373–380. doi:10.1061/(asce)1090-0241(2004)130:4(373).

[37] Burns, B., Barker, R., & Ghataora, G. S. (2006). Investigating internal erosion using a miniature resistivity array. NDT & E International, 39(2), 169–174. doi:10.1016/j.ndteint.2004.12.009.

[38] Briaud, J. L., Ting, F. C. K., Chen, H. C., Cao, Y., Han, S. W., & Kwak, K. W. (2001). Erosion Function Apparatus for Scour Rate Predictions. Journal of Geotechnical and Geoenvironmental Engineering, 127(2), 105–113. doi:10.1061/(asce)1090-0241(2001)127:2(105).

[39] Marot, D., Regazzoni, P.-L., & Wahl, T. (2011). Energy-Based Method for Providing Soil Surface Erodibility Rankings. Journal of Geotechnical and Geoenvironmental Engineering, 137(12), 1290–1293. doi:10.1061/(asce)gt.1943-5606.0000538.

[40] Chang, D. (2012). Internal erosion and overtopping erosion of earth dams and landslide dams. Ph.D. Thesis, Hong Kong University of Science and Technology, Hong Kong.

[41] Chevalier, C., Haghighi, I., & Herrier, G. (2012). Resistance to erosion of lime treated soils: a complete parametric study in laboratory. Proceedings of the 6th International Conference on Scour and Erosion, 27-31 August, Paris, France.

[42] de Baecque, M., Chevalier, C., Palma-Lopes, S., Le Feuvre, M., Reiffsteck, P., Charles, I., & Herrier, G. (2017). Resistance to erosion of lime treated soils for application to coastal dikes. 25th meeting of the European Working Group on Internal Erosion in Embankment Dams and their Foundations, 4-7 September, 2017, Delft, Netherlands.

[43] Haghighi, I., Chevalier, C., Duc, M., Guédon, S., & Reiffsteck, P. (2013). Improvement of Hole Erosion Test and Results on Reference Soils. Journal of Geotechnical and Geoenvironmental Engineering, 139(2), 330–339. doi:10.1061/(asce)gt.1943-5606.0000747.

[44] Říha, J., & Jandora, J. (2014). Pressure conditions in the hole erosion test. Canadian Geotechnical Journal, 52(1), 114–119. doi:10.1139/cgj-2013-0474.

[45] Mehenni, A., Cuisinier, O., & Masrouri, F. (2016). Impact of Lime, Cement, and Clay Treatments on the Internal Erosion of Compacted Soils. Journal of Materials in Civil Engineering, 28(9). doi:10.1061/(asce)mt.1943-5533.0001573.

[46] Fattahi, S. M., Soroush, A., & Shourijeh, P. T. (2017). The hole erosion test: A comparison of interpretation methods. Geotechnical Testing Journal, 40(3), 494–505. doi:10.1520/GTJ20160069.

[47] Royal, A. C. D., Opukumo, A. W., Qadr, C. S., Perkins, L. M., & Walenna, M. A. (2018). Deformation and Compression Behaviour of a Cement–Bentonite Slurry for Groundwater Control Applications. Geotechnical and Geological Engineering, 36(2), 835–853. doi:10.1007/s10706-017-0359-9.

[48] Opdyke, S. M., & Evans, J. C. (2005). Slag-Cement-Bentonite Slurry Walls. Journal of Geotechnical and Geoenvironmental Engineering, 131(6), 673–681. doi:10.1061/(asce)1090-0241(2005)131:6(673).

[49] Walenna, M. A. (2023). Investigating the Consolidation Behaviour of Cement-Bentonite Barrier Materials Containing PFA and GGBS. Civil Engineering Journal (Iran), 9(3), 512–530. doi:10.28991/CEJ-2023-09-03-02.

[50] TOLSA. (2008). Technical Data Sheet: Berkbent Bentonite 163. TOLSA, Madrid, Spain.

[51] BS EN 197-1. (2019). Cement - Composition, specifications and conformity criteria for common cements. British Standard Institution, London, United Kingdom.

[52] Royal, A. C. D., Makhover, Y., Moshirian, S., & Hesami, D. (2013). Investigation of Cement-Bentonite Slurry Samples Containing PFA in the UCS and Triaxial Apparatus. Geotechnical and Geological Engineering, 31(2), 767–781. doi:10.1007/s10706-013-9626-6.

[53] Jefferis, S. (2012). Cement-Bentonite Slurry Systems. Proceedings of the Fourth International Conference on Grouting and Deep Mixing, February 15-18, 2012, 1–24. doi:10.1061/9780784412350.0001.

[54] Ke, L., & Takahashi, A. (2014). Experimental investigations on suffusion characteristics and its mechanical consequences on saturated cohesionless soil. Soils and Foundations, 54(4), 713–730. doi:10.1016/j.sandf.2014.06.024.

[55] Fan, H., Dhir, R. K., & Hewlett, P. C. (2021). GGBS Use in Concrete as Cement Constituent: Strength Development and Sustainability Effects-Part 1. Magazine of Concrete Research, 1–41. doi:10.1680/jmacr.21.00009.

[56] Munjal, P., Hau, K. K., & Hon Arthur, C. C. (2021). Effect of GGBS and curing conditions on strength and microstructure properties of oil well cement slurry. Journal of Building Engineering, 40, 102331. doi:10.1016/j.jobe.2021.102331.